



## Design and Analysis of Revolutionary Elevated Supersonic Axial Turbines

Nadupuru Bhaskara Rao<sup>1</sup>, Rajesh CVS<sup>2</sup>, Uppada Komali<sup>3</sup>

<sup>1,2,3</sup>Assistant Professor, Department of Mechanical Engineering,

<sup>1,2</sup>Vizag Institute of Technology, Visakhapatnam, Andhra Pradesh, India

<sup>3</sup>Bhimavaram Institute of Engineering & Technology, Andhra Pradesh, India

### ABSTRACT

The improvement in ultra compact thermal power creation is constrained by the unavailability of fluid machinery sufficient for supersonic flow circumstances. Conservative turbine designs exhibit unacceptable performances related to large aerodynamic losses and a narrow operation range. This paper provides for the first time in the open literature the design procedure, and subsequent analysis of the turbine performance of a turbine satisfactory for supersonic axial pulsating flows, as those encountered in pioneering combustors. The design comes up to consider the most adverse condition, a steady inlet axial Mach number equal to 3.5. The possible turbine families were classified by the velocity triangles and discussed. An elementary issue in supersonic passages is to ensure the normal shock at the start of the engine is swallowed through the turbine passages, namely the turbine passage is started. To ensure self starting capability the turning is restricted to lower values than in the conventional subsonic turbines. The design procedure was based on the method of characteristics, converting the inlet uniform flow into a vortex flow field, such that the adequate deflection is inflicted to the supersonic flow. The presentation of the supersonic passage was first assessed and then compared to conservative designs. The present design procedure and analysis of unconventional supersonic turbines provides strategy for the plan and optimization of efficient elevated supersonic passages, fit to future tightly packed fluid machinery.

### INTRODUCTION

The thermal efficiency of highly developed mutual cycles surpasses 62.8%, allowing for a turbine opening temperature of 1703 K [1]. However, the

maximum possible efficiency offered by the Carnot cycle for the same firing temperature would be 82.8%. While further increase in pressure ratios and firing temperature gradually enhance the cycle efficiency, novel turbine-based thermal plants offer a potential leap in efficiency. In particular, the Humphrey and Fickett–Jacobs cycles provide a rise of pressure through the combustion process. Fig. 1a and b display the entropy–enthalpy and pressure–volume charts of the ideal Joule–Brayton (constant pressure heat addition), the Humphrey, and the Fickett–Jacobs cycles. The Humphrey cycle is based on constant volume heat addition with an isentropic expansion and an isobaric heat rejection. In the Fickett–Jacobs cycle, the combustion is an explosive process, utilized in the 1920s in a Hozwarth turbine [2], or using perhaps a special piston-cylinder arrangement, that in practice results in supersonic flow conditions at the combustor exit. A multitude of research teams have suggested the use of pressure gain combustion for power plants [3]. The use of a constant volume combustor, displayed in red in Fig. 1a and b, allows achieving the same time-averaged combustor exit temperature at a higher-pressure level (the turbine inlet temperature  $T_4$  is fixed by the current material technology). Conversely, to achieve the same turbine inlet conditions of a Joule cycle, the Humphrey cycle requires less pressure increase in the compressor. Consequently, the Humphrey cycle offers a potential surge in specific power and cycle efficiency. Nevertheless to achieve the potential gain in such pioneering power plant, the turbine efficiency should be above a certain threshold dictated by the combustor pressure rise and turbine entry temperature. Let us consider that the Joule engine is equipped with a 90% efficiency turbine, Fig. 1c demonstrates that the

required efficiency of the turbine in the Humphrey cycle to achieve the same cycle efficiency than the Joule cycle, decreases a function of the combustor pressure rise. Humphrey cycles operating at large turbine entry temperatures, with low compression ratio require low turbine efficiencies. For instance, in a Humphrey cycle with  $T_4 = 1500$  K,  $P_3/P_2 = 5$ ; with a combustor pressure rise of 40%, a turbine with an isentropic efficiency of 59% would extract the same work than a 90% efficiency turbine in a Joule cycle.

**Nomenclature**

- A Area [m<sup>2</sup>]
- C Chord [m]
- E Relative error
- M Mach number  $V / (\gamma \cdot R \cdot T)^{1/2}$
- R Grid refinement factor
- 1,2 Inlet and outlet conditions of a stator row, respectively
- 2,3 Inlet and outlet conditions of a rotor row, respectively

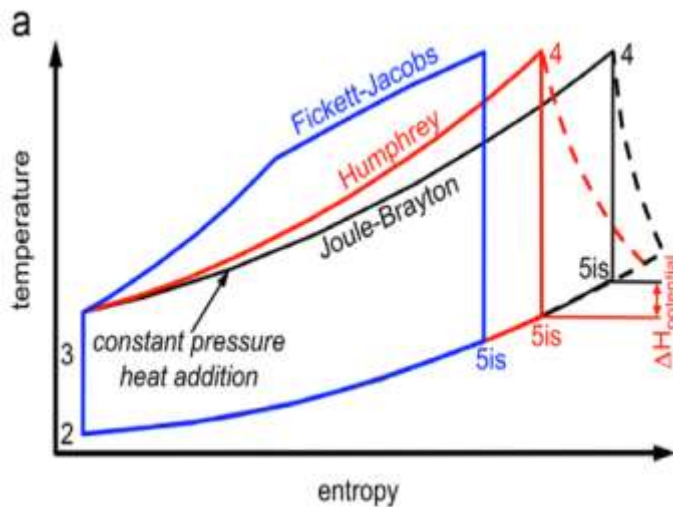
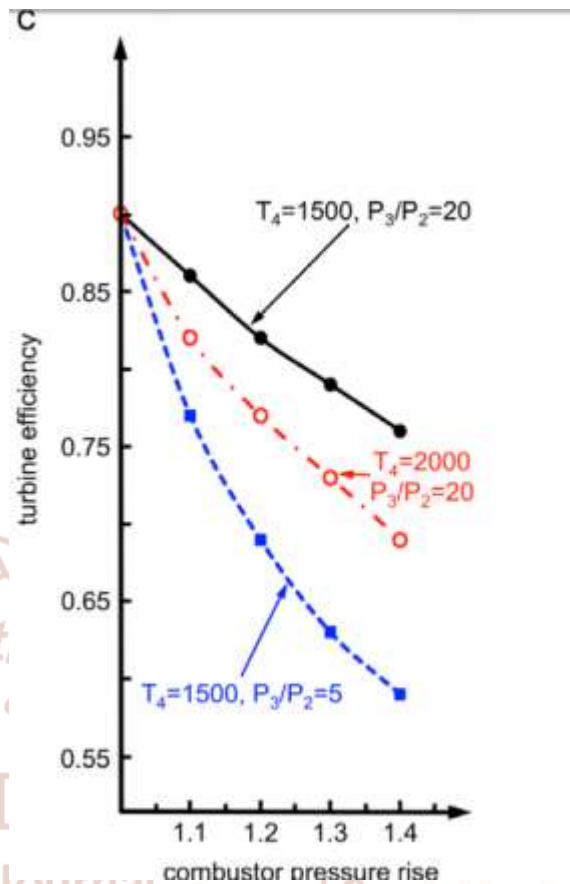
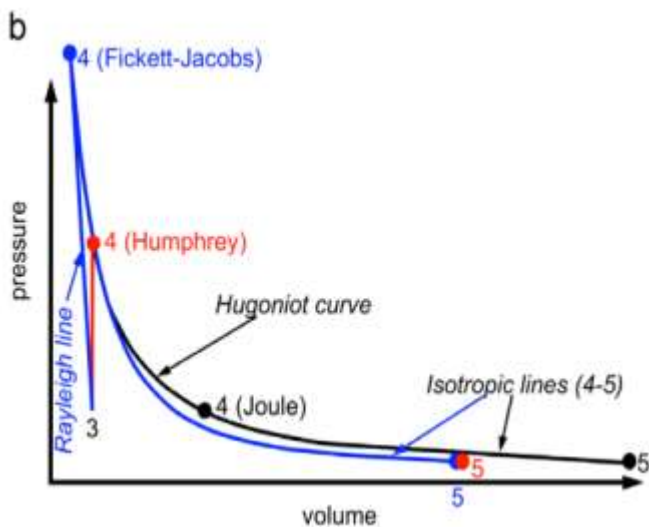


Figure-1 indicate the Single closed loop cycles: a) Simplified enthalpy entropy representation; b) Pressure-volume layout; c) Turbine efficiency in a Humphrey cycle to obtain the same efficiency than a Brayton cycle with a 90% turbine efficiency. (For interpretation of the references to color in this figure, the reader is referred to the web version of this article.)



**Supersonic passage designs**

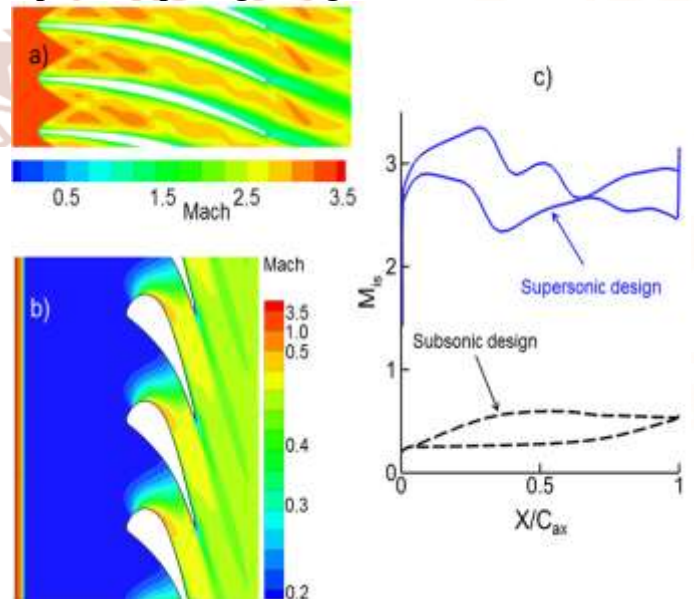
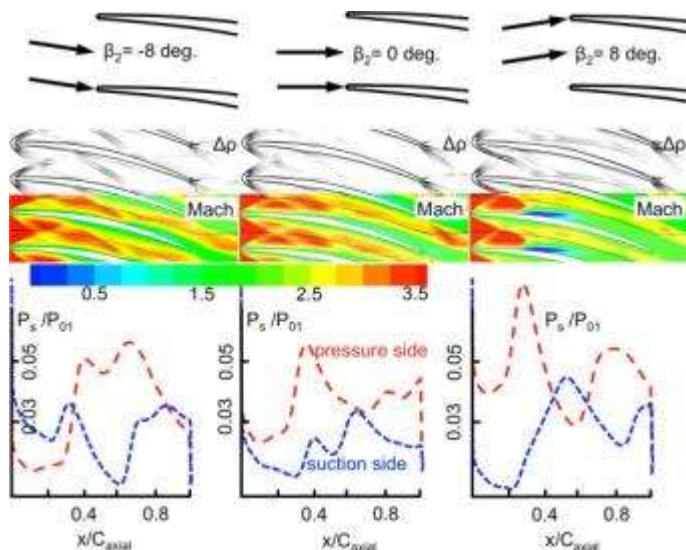
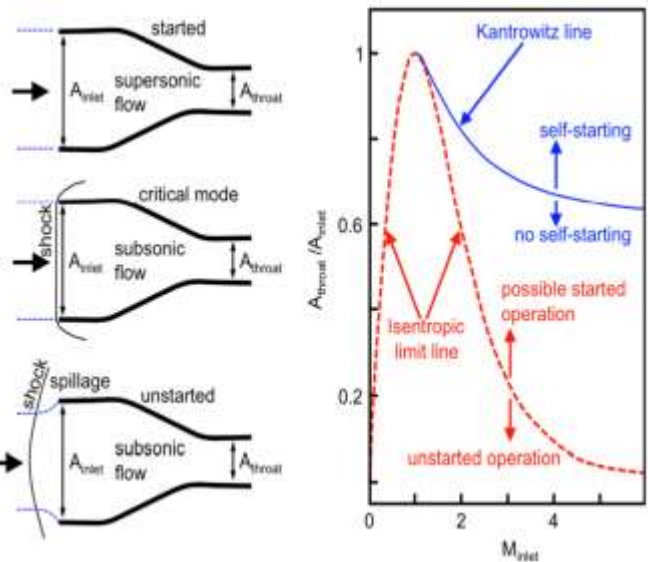


Figure-2



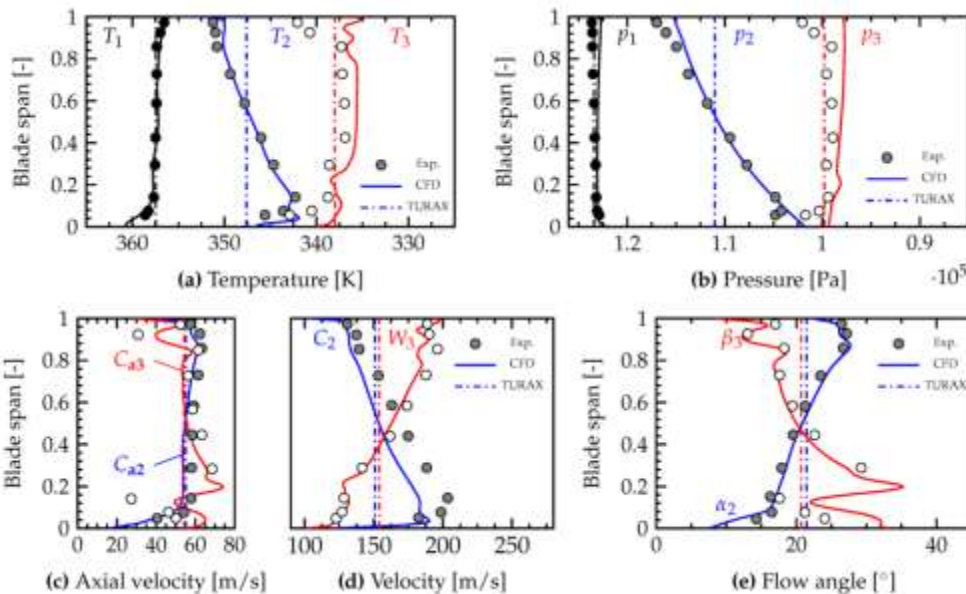
Above figure shows a passage designed with the “corner flow method”. The front suction side is curved to cancel the incoming compression waves generated along the concave pressure side, followed then by a parallel flow. The flow subsequently experiences a corner flow expansion, where waves are canceled by the concave surface, until uniform parallel flow is achieved at the exit. However, the design exhibits zero loading in the central part of the passage, and the flow turning is limited.

Possible in take operating regions shown in Figure3 below,



Supersonic turbines have attracted interest from the industry since the 1950s due to the high specific power they could provide, allowing a reduction in the number of low-pressure stages, and thus leading to lighter turbines together with lower manufacture and operational costs.

Fig. 2 a depicts three distinct regions in the vane nozzle: a converging (subsonic) section, a diverging (supersonic) section and a straight section in the rear suction surface. To maximize the specific power, the degree of reaction is traditionally very low. The design of such impulse type rotors can be achieved following two different strategies based on the method of characteristics

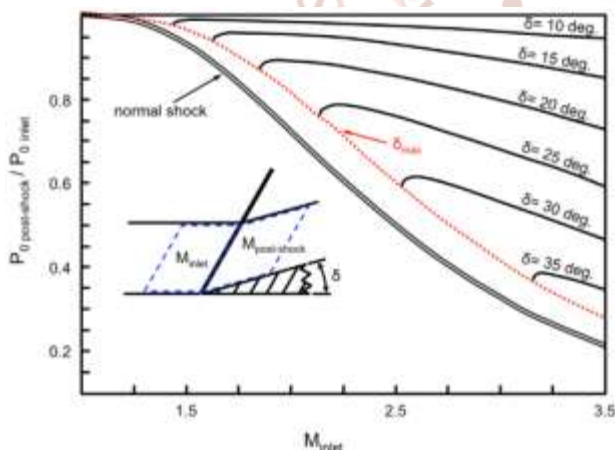
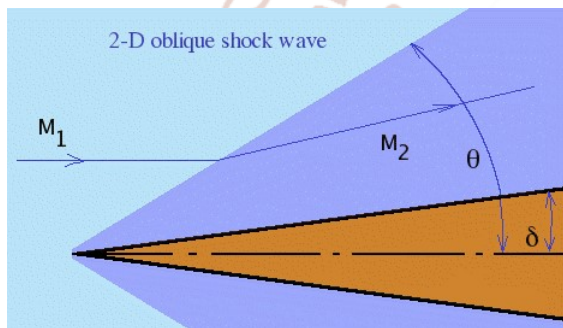


State-of-the-art high-pressure-turbine vane passages are characterized by a strong area contraction up to the throat. Consequently, when conventional vanes are exposed to high supersonic inlet Mach numbers

the diffuser is never self-starting. Standing shock waves upstream of the turbine cascade cause large irreversibilities and, in particular, abatement of the dynamic pressure,

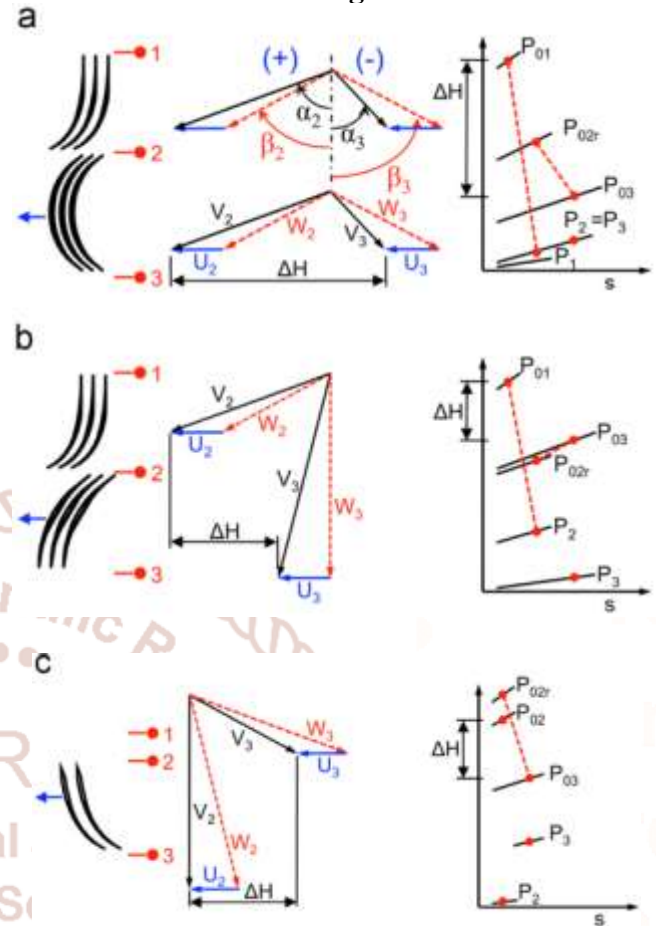
An additional problem is the unfavorable pressure gradient across supersonic diffusers that may lead to boundary layer separation, which additionally limits flow turning in the passage. Furthermore, the efficiency of a supersonic turbine is seriously penalized by the existence of flow separation on the suction surface caused by shock–boundary layer interactions. Higher loadings, i.e. higher suction surface Mach numbers and lower pressure surface Mach numbers are desirable for the starting condition as well as to maximize the work produced by the turbine. However, adverse pressure gradients will become much more pronounced within the passage, clearly showing an important compromise between starting conditions and flow separation.

The current paper presents an approach to design turbine passages with adequate contraction area ratios. The performance of these unconventional turbine passages was evaluated numerically using the solver CFDp, both in steady and transient operation, to study the movement of a normal shock wave across the turbine.



The fundamental purpose of the present research is to provide guidelines to designers of an unprecedented family of turbine passages suitable for supersonic applications. In addition, the performance analysis of the components is needed to assess the potential performance gain of novel thermal cycles operating with internal supersonic flows.

### Procedure of Turbine Design



Above figure

Displays all the possible turbine configurations considering an axial supersonic inlet flow, the velocity triangles and the associated entropy enthalpy diagrams, Considering adiabatic conditions, without cooling, the turbine channel outlet static conditions can be evaluated using the compressible flow equations, diffusing channel, and a reaction concept as sketched in above figure with a rotor nozzle design. The work extraction is maximum for a vane outlet swirl equals to 671 and rotor turning equals to 1161 ( $\beta_2^{1/4}\beta_3^{1/4}581$ ), implying no velocity change across the rotor passage if there were no shock losses. This impulse design (above figure) delivers a high outlet swirl, and both stator and rotor passages experience diffusion. In the rotor relative frame of reference, due to the upstream stator and peripheral velocity of the passage, inlet swirl to the rotor is present; hence flow acceleration is possible across the rotor passage. above figure depicts the velocity triangle of a turbine that comprises rotor passages with flow acceleration (nozzle type). Such a design would be the most benign for the rotor aerodynamics; however the work extraction is limited. An alternative solution, with a similar work extraction, would be to consider a stator

less configuration, as sketched in above figure the rotor is diffusing the flow, but such a concept offers numerous advantages, particularly a reduction in the number of components. In the following the design is concerned with either the stator geometry displayed in Fig. 5a and b or the rotor of above figure.

$$\frac{A_{throat}}{A_{inlet}} = \frac{1}{M_{inlet}} \left( \frac{2(1+(\gamma-1)/2)M_{inlet}^2}{\gamma+1} \right)^{-(\gamma+1)/(2(\gamma-1))} \quad (1)$$

$$M_2^2 = \frac{(\gamma-1)M_{inlet}^2 + 2}{2\gamma M_{inlet}^2 - (\gamma-1)} \quad (2)$$

corresponding to a stator or rotor passage by applying the mass conservation principle:

$$\frac{\dot{m} \sqrt{C_p T_0}}{A_n P_0} = \frac{\gamma}{\sqrt{\gamma-1}} M \left( 1 + \frac{\gamma-1}{2} M^2 \right)^{-(\gamma+1)/(2(\gamma-1))} \quad (3)$$

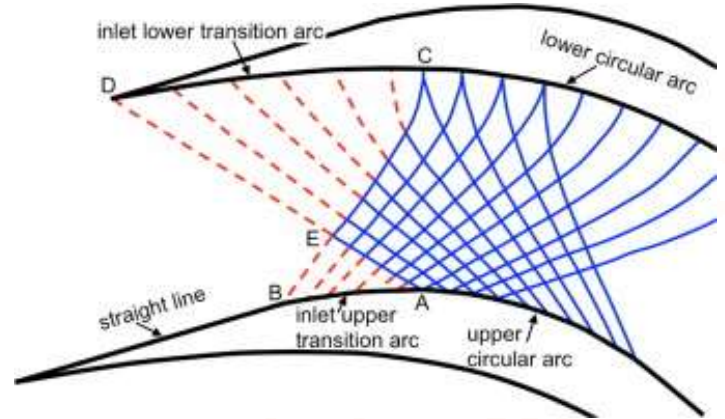
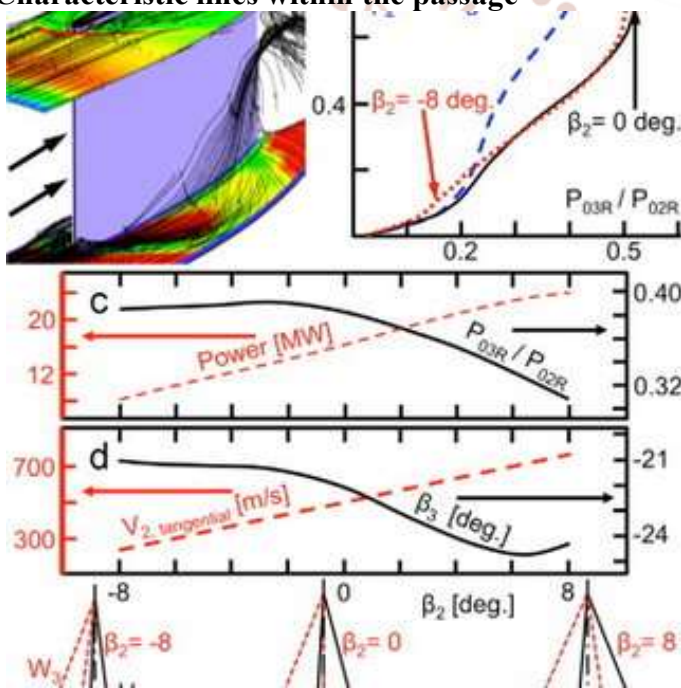
Within an axial turbo machine the pitch ( $g$ ) is constant, assuming a constant channel height ( $H$ ), the area ratio inlet to any station ( $A_n/A_{inlet}$ ) can be expressed according to the following expression Eq. (4):

$$\frac{A_n}{A_{inlet}} = \frac{H \cdot g \cdot \cos(\alpha_n)}{H \cdot g \cdot \cos(\alpha_{inlet})} = \frac{\cos(\alpha_n)}{\cos(\alpha_{inlet})} \quad (4)$$

Neglecting pressure losses and assuming constant flow properties, the mass flow conservation across the passage yields the outlet Mach number ( $M_{outlet}$ ) as a function of the inlet Mach number ( $M_{inlet}$ ) and the passage turning as shown by Eq. (5). For a stator the equation is terms of the absolute angle ( $\alpha_{outlet} - \alpha_{inlet}$ ), while for a rotor the turning would be expressed in the relative frame of reference ( $\beta_{inlet} - \beta_{outlet}$ ):

$$\left( 1 + \frac{\gamma-1}{2} M_{inlet}^2 \right)^{-(\gamma+1)/(2(\gamma-1))} M_{inlet} \cos \alpha_{inlet} = \left( 1 + \frac{\gamma-1}{2} M_{outlet}^2 \right)^{-(\gamma+1)/(2(\gamma-1))} M_{outlet} \cos \alpha_{outlet} \quad (5)$$

**Characteristic lines within the passage**



This value represents the angle through which the flow must turn from  $M=1$  to the required Mach number.

$$v = \frac{\pi}{4} \left( \sqrt{(\gamma+1)/(\gamma-1)} - 1 \right) + \frac{1}{2} \left\{ \sqrt{(\gamma+1)/(\gamma-1)} \sin^{-1} \left[ (\gamma-1)M^{*2} - \gamma \right] + \sin^{-1} \left( \frac{\gamma+1}{M^{*2} - \gamma} \right) \right\} \quad (6)$$

The critical velocity ratio  $M^*$  is expressed by the following relation Eq. (7):

$$M^* = \left( \frac{M^2(\gamma-1)/2}{1 + M^2(\gamma-1)/2} \right)^{1/2} \quad (7)$$

The circular arcs are designed to maintain the vortex flow field region, where the flow velocity is inversely proportional to the radius:

$$V R = \text{constant} \quad (8)$$

Therefore, the pressure and suction side Mach numbers remain constant along the vortex region. When normalizing Eq. (8) by the critical velocity ( $V_{critical}$ ) and the correspondent radius of the sonic velocity streamline ( $r^*$ ) it can be re-written with dimensionless parameters (at  $R=r^*$ ,  $V=V_{critical}$ ):

$$M^* \cdot R^* = 1 \quad (9)$$

Where  $R^*=R/r^*$  is the dimensionless radius of the vortex flow field and  $M^*=V/V_{critical}$  is the dimensionless velocity. Once the designer specifies the values for  $v_{upper}$  and  $v_{lower}$ , the values of  $M_{upper}^*$  and  $M_{lower}^*$  are fixed and  $R_{upper}^*$  and  $R_{lower}^*$  can be determined with Eq. (9). Considering  $\beta_{inlet}$  and  $\beta_{outlet}$  as the inlet and outlet flow angles respectively, the amount of turning in the circular arcs region are defined by Eq. (10).

$$\begin{aligned} \alpha_{lower,inlet} &= \beta_{inlet} - (v_{inlet} - v_{lower}) \\ \alpha_{lower,outlet} &= \beta_{outlet} - (v_{outlet} - v_{lower}) \\ \alpha_{upper,inlet} &= \beta_{inlet} - (v_{upper} - v_{inlet}) \\ \alpha_{upper,outlet} &= \beta_{outlet} - (v_{upper} - v_{outlet}) \end{aligned} \quad (10)$$

In order to fully define the circular arcs, the outlet flow angle  $\beta_{outlet}$  is determined with Eq. (5), for a selected outlet Mach number ( $M_{outlet}$ ). Since the starting and terminal points are known, the circular arcs are now fully defined. The design of the lower transitional arcs is performed with respect to non-dimensional axes  $x^* = x/r^*$  and  $y^* = y/r^*$ . The arcs are designed in a marching manner by adding straight wall segments that produce a small change in the flow angle and the respective variation in the Mach number. According to [12] the velocity direction ( $\varphi$ ) can be written in function of the dimensional radius.

$$\varphi = \pm \frac{1}{2}f(R^*) + const. \tag{11}$$

$$f(R^*) = \sqrt{(\gamma+1)/(\gamma-1)} \sin^{-1} \left( \frac{(\gamma-1)}{R^{*2}} - \gamma \right) + \sin^{-1}((\gamma-1)R^{*2} - \gamma) \tag{12}$$

The positive sign in Eq. (11) stands for the expansion lines, while the negative sign represents the compression lines. Applying a known boundary condition at  $x^* = 0$  where  $\varphi=0$  and  $R^* = R_{lower}^*$ , the equation for the expansion lines is defined by Eq. (13).

$$\varphi = \frac{1}{2}[f(R^*) - f(R_{lower}^*)] \tag{13}$$

Considering now the discretization of the transition arc into  $k$  segments where each one turns the flow in  $\Delta v$  degrees it is possible to determine the direction of each one of them with Eq. (14).

$$\varphi_{k,inlet} = v_{inlet} - v_{lower} - (k-1)\Delta v \tag{14}$$

This definition of  $\varphi$  can now be used in Eq.(13):

$$f(R_k^*) = 2v_{inlet} - 2(k-1)\Delta v - 2v_{lower} + f(R_{lower}^*) \tag{15}$$

Substituting now the two last terms into Eqs. 6 and 12, the value of  $f(R_k^*)$  becomes only in function of the dimensionless radius and the incremental flow turning as shown in Eq. (16).

$$f(R_k^*) = 2v_{inlet} - 2(k-1)\Delta v - \left( \frac{\pi}{2} \sqrt{(\gamma+1)/(\gamma-1)} - 1 \right) \tag{16}$$

Eqs. 12 and 17 allow the determination the values of  $R_k^*$  and  $\varphi_k$ . Hence for each  $k$  increment its coordinates can be determined with Eq. (17).

$$x_{k,inlet}^* = -R_{k,inlet}^* \sin \varphi_{k,inlet}^* \tag{17}$$

$$y_{k,inlet}^* = R_{k,inlet}^* \cos \varphi_{k,inlet}^*$$

Each segment of the transitional arc is a straight line parallel to the velocity direction  $\varphi_k$ , therefore the slope of the wall  $m_k$  can be computed with Eq. (18)

$$m_{k,inlet} = \tan \varphi_{k+1,inlet}^* \tag{18}$$

Finally the equation of the wall segment can be determined, where  $k$  varies from 1 to  $k_{max} = (v_r - v_t) / \Delta v$ .

$$y^* = m_{k,inlet} [x^* - (x_{lower}^*)_{k+1,inlet}] + (y_{inlet}^*)_{k+1,inlet} \tag{19}$$

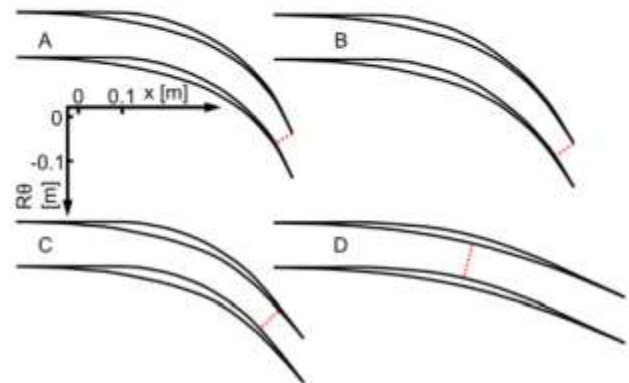
The design methodology of the upper transitional arc is analogous to the one used for the lower transitional arc. At the outlet of the passage the procedure is reversed to achieve the uniform outlet Mach number ( $M_{outlet}$ ). The remainder of the airfoil design is thereby completed with the use of straight lines, on the suction surface, parallel to the flow direction.

**Table 1**  
Inlet conditions to the supersonic passage.

$M_{inlet}$	3.5
$\alpha_{inlet}$ [deg]	0.0
$P_{0\ inlet}$ [bar]	40
$P_s\ inlet$ [bar]	0.52
$T_s\ inlet$ [K]	725

**Table 2**  
Supersonic passages outlet properties.

	$M_{outlet}$	$P_s\ outlet$ [bar]	$\alpha_{\beta_{outlet}}$ [deg]	$\beta_{upper}$ [deg]	$\beta_{lower}$ [deg]	$A_{throat}/A_{inlet}$
A	2.5	2.3	67	82	38	0.45
B	2.8	1.5	59	74	40	0.52
C	3.0	1.1	51	78	38	0.61
D	3.4	0.6	24	66	46	0.80

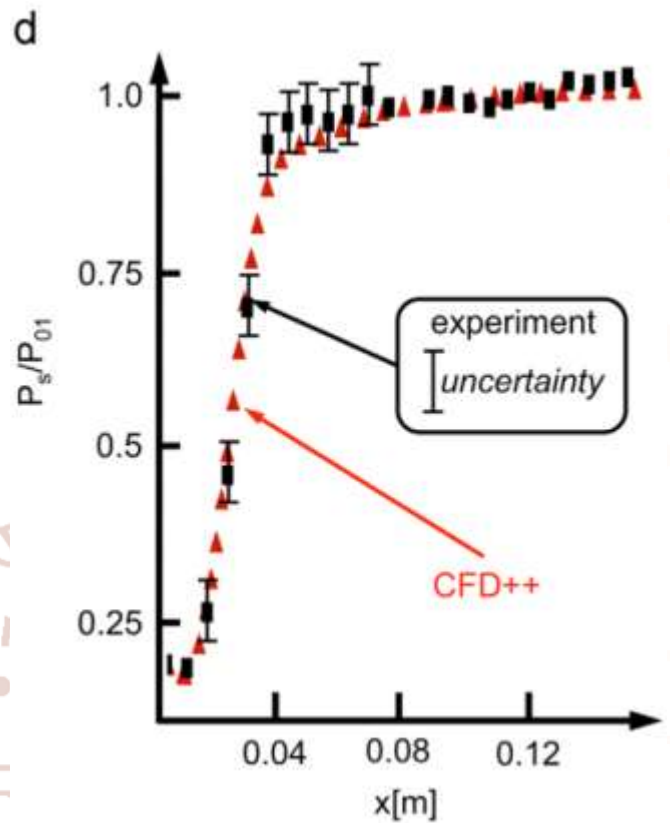
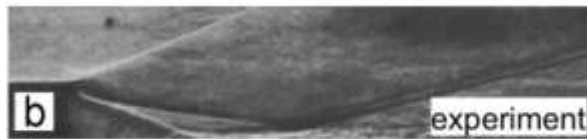
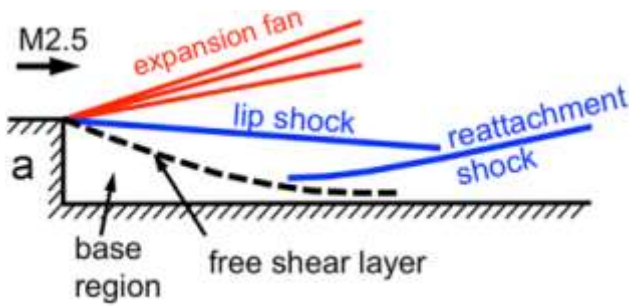


The sharp airfoils A, B, C, and D, with the throats marked with red dotted lines. For in terpretation of the references to color in this figure legend,

The above figure shows the geometry of the four different passages. In cases A and B, the throat is located at the trailing edge, while for airfoils C and D the throat is located upstream. The numerical simulations demonstrated that for all geometries a constant Mach number region exists as defined with the design approach based on the Method of characteristics. Reducing the turning (from airfoil A to airfoil D) we decrease the pressure loading on the airfoil and the contraction ratio. In this research the airfoil height was kept constant in order to focus on the 2D blade-to-blade analysis and ease the practical implementation in a stator row (with a given diameter) and control the tip radius in a rotating row. Consequently, airfoil D was selected to ensure self-starting of the passage during the testing of the cascade from no-flow into the supersonic regime.

**Table 3**  
Turbine passage design characteristics.

Number of airfoils	23		
Height [m]	0.050		
	hub	mid-span	tip
Chord [m]	0.562	0.562	0.562
Axial chord [m]	0.550	0.550	0.550
Inlet radius [m]	0.345	0.370	0.392
Outlet radius [m]	0.345	0.370	0.392
Pitch [m]	0.094	0.101	0.108
Throat [m]	0.075	0.081	0.086
Trailing edge thickness [m]	0.005	0.005	0.005

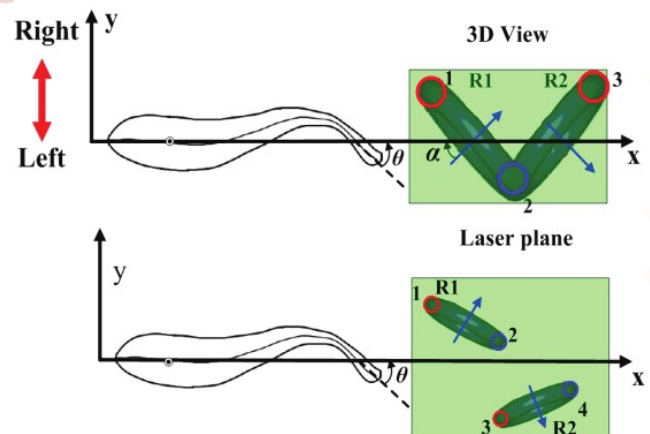
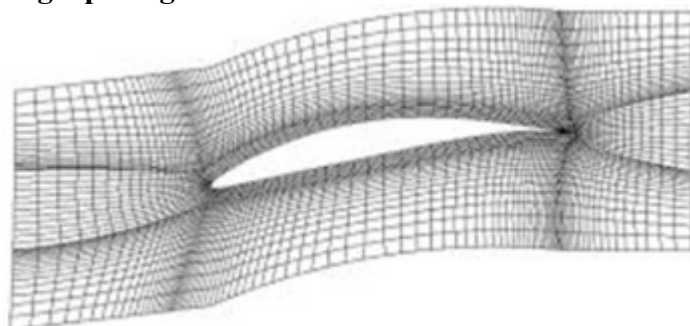


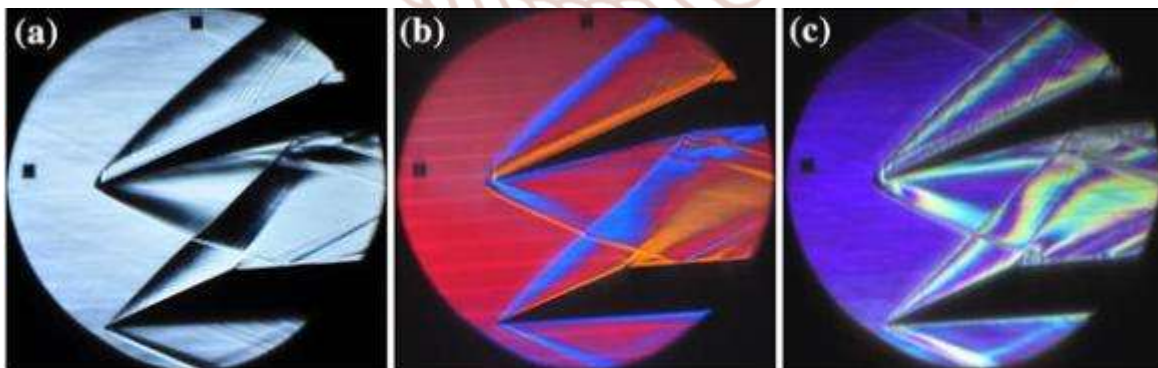
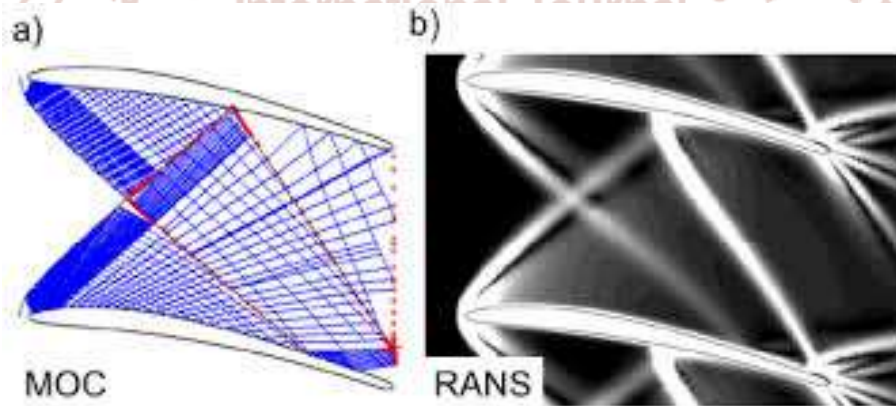
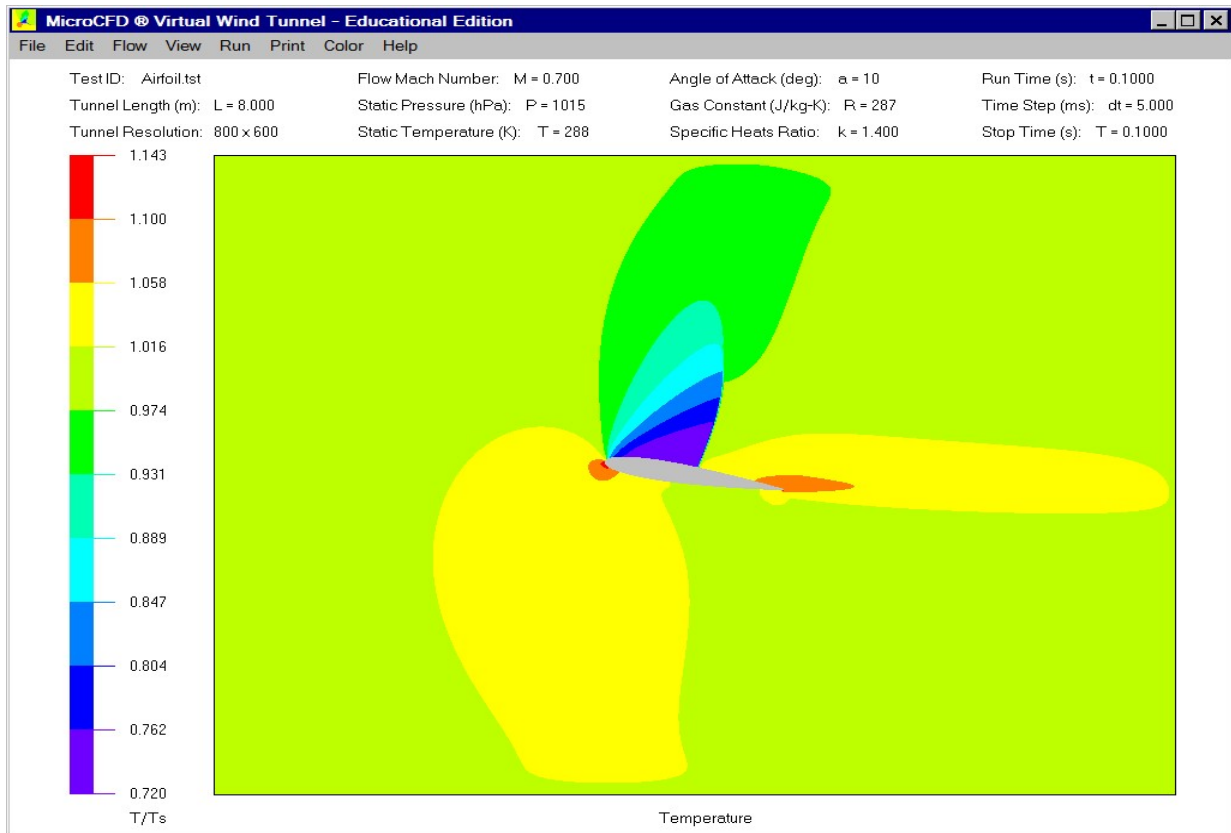
(a) Main flow features in the supersonic backward facing step, (b) experimental shadowgraph [19], (c) shadowgraph obtained with CFD++ and (d) static pressure distribution downstream of the backward facing step.

**Table 4**  
Results of grid sensitivity analysis.

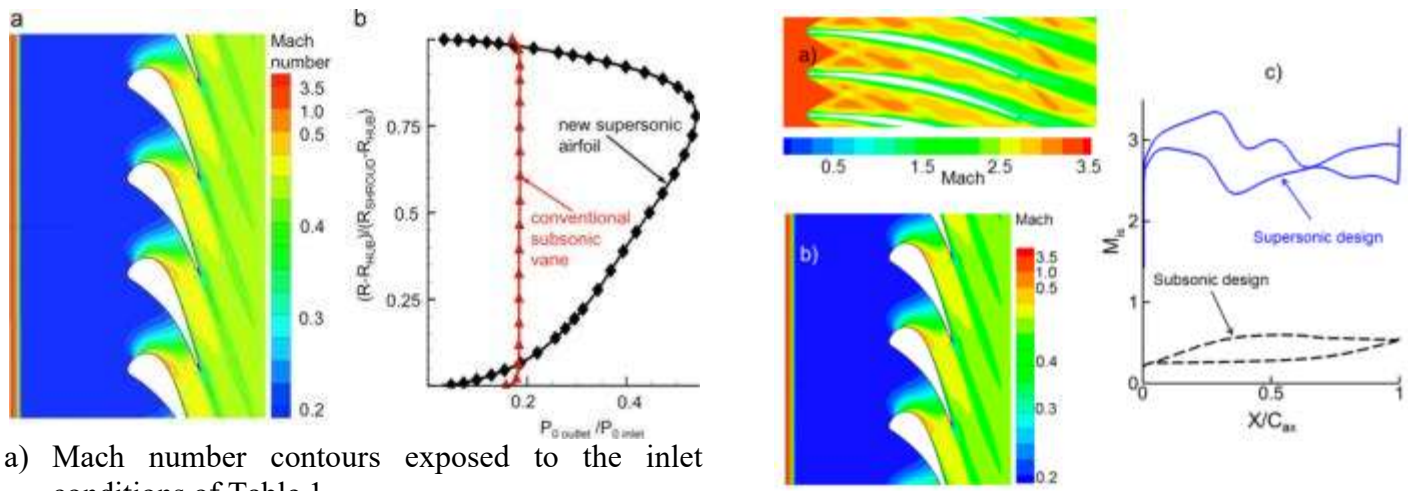
	$\phi = P_{0, outlet} / P_{0, inlet} [-]$	$\phi = M_{outlet} [-]$	$\phi = P_{t, outlet} [Pa]$
$N_{fine} / N_{medium} / N_{course}$	6,215,398 / 2,117,502 / 721,966		
$r_{medium-fine} / r_{course-medium}$	1.43 / 1.43		
$\phi_{fine} / \phi_{medium} / \phi_{course}$	0.42 / 0.41 / 0.41	2.29 / 2.28 / 2.27	118,570 / 118,621 / 119,309
$p$	4.34	2.04	7.26
$\phi_{medium-fine}$	0.42	2.30	118,566
$\phi_{medium-fine}$	2.60%	0.57%	0.04%
$\phi_{medium-fine}$	0.69%	0.53%	0.00%
$GCI_{medium-fine}$	0.87%	0.66%	0.00%

Topology of the structural blocks used to mesh a single passage





Schlieren images of an expansion fan/shock wave interaction with a Mach 2.5 freestream and the cut-offs oriented parallel to the freestream: a) knife edge, b) tri-colour mask, and c) band lattice mask



a) Mach number contours exposed to the inlet conditions of Table 1  
 b) Distributions of outlet to inlet total pressure ratio.

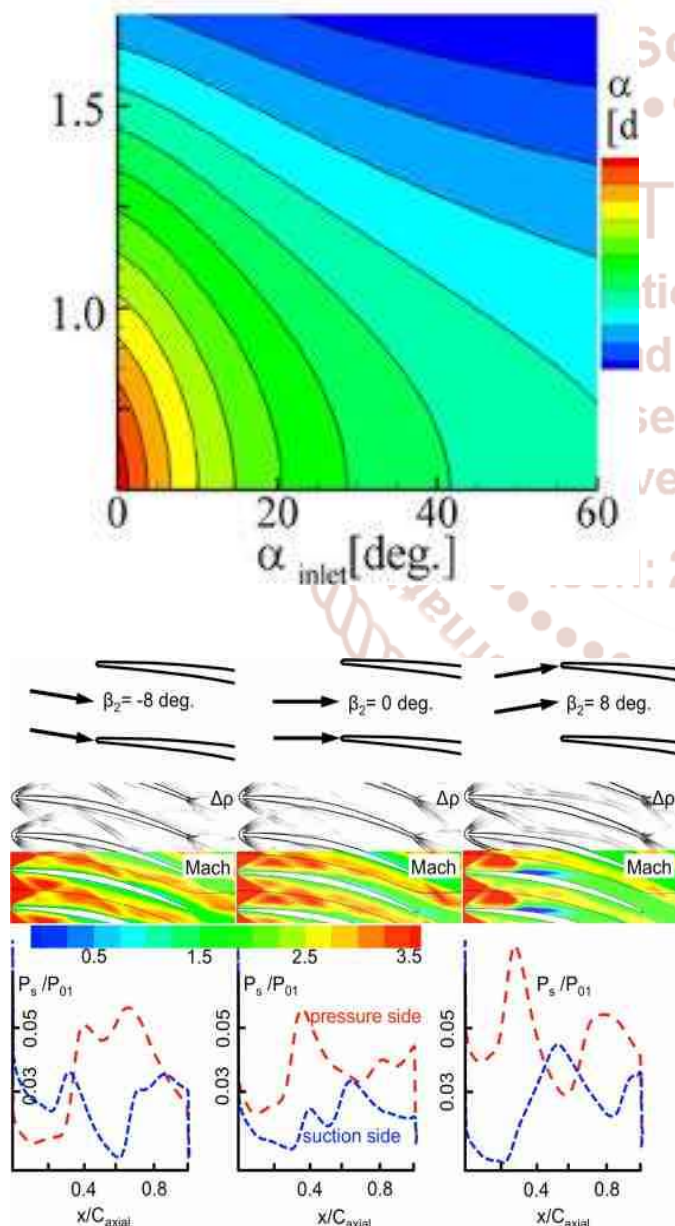
**Results and Discussion**

The mathematical Schlieren visualization displayed in above figures illustrates the complex shock patterns across the turbine passage. The two oblique shock waves generated at the leading edge interact with the boundary layers of the neighboring airfoils, and are reflected multiple times further downstream. Above figures depicts the static pressure distribution along the airfoil, which is characterized by the strong fluctuations on the pressure and suction side imposed by the impact of the direct and reflected shock waves.

From the above figures shows the distortion in the Mach number field generated by the leading-edge shocks. Due to the passage area reduction and pressure losses, the passage outlet Mach number is reduced to 2.15, while the isentropic prediction (Table 2) stated a value of 3.4. The leading edge shocks and their interactions with the airfoil boundary layer cause substantial total pressure losses along the turbine.

Near the end-walls, extremely high total pressure losses were registered, in the boundary layers and vertical structures occurring in those regions. Moving towards the mid-span, total pressure losses are reduced, due to the decreased importance of secondary flows.  $P_0$  outlet/ $P_0$  inlet reaches its maximum mass-weighted average value of 54% at a normalized radius  $(R_{RhUB}) / (R_{tipRhUB})$  of approximately 0.78. At the outlet section of the computational domain, the mass flow-weighted averaged value for  $P_0$  outlet / $P_0$  inlet is 34%.

The performance of a stator less turbine was numerically assessed considering as a rotor the turbine passage previously designed. The relative inlet angle, at design conditions, is zero, but we studied eight other off-design cases, with a variation in  $\beta_2$



781. In all cases we considered identical relative inlet total pressure (40 bar), inlet relative Mach number 3.5, and that the rotor turns at 12,910 RPM, resulting in  $U_{2\frac{1}{4}500}$  m/s. Hence, the total inlet conditions in the absolute frame of reference (P01 and T01) increase with the relative inlet angle.

The above figure evaluates the pressure distribution on the turbine passage with the aid of Schlieren and iso-Mach number contours, at negative incidence (left column), design (central column), and positive incidence (right column). At negative incidence ( $\beta_{2\frac{1}{4}} 8$ ) there are two concurrent effects. Firstly, the acceleration along the pressure side (in red) is enhanced, and consequently negative loading is observed in the front part of the airfoil. This is coupled with a weak right-running leading edge shock. At about 35% of the axial chord the left-running shock from the neighboring leading edge impacts on the pressure side, increasing the loading substantially above the suction side level. At around 25% of the axial chord the weak right-running shock from the other neighboring leading edge impacts on the suction side. By contrast, the strong leading-edge left-running shock is reflected on the pressure side, and then impacts again on the suction side at about 65% of the axial chord. Consequently, the pressure levels at the suction side approaches the value at the pressure side; such low difference creates a weak trailing edge right running shock [22]. At positive incidence angles ( $\beta_{2\frac{1}{4}} 8$ ), the effects at the leading edge are reversed, i.e. a steeper acceleration along the suction side (in blue) is coupled with a strong right-running leading edge shock. This intense right-running shock impacts on the suction side at about 30% of the axial chord, originating a bubble of recirculating flow that is clearly identified by the blue region in the iso-Mach contour. This separation region is eventually reattached to the suction side, and from 50% of the axial chord, the flow is again accelerated along the suction side.

### Conclusion

Present investigate on groundbreaking thermodynamic cycle's has shown an unacceptable performance of the conventional turbine devices. The present research has shown that conventional subsonic turbine designs are inadequate for supersonic conditions, due to the generation of an intense normal shock wave at the inlet. The proposed supersonic passages were designed using a methodology based on the method of characteristics. The turbine passage

is comprised of three zones which, (i) convert the uniform parallel flow at the passage inlet into a vortex flow field, (ii) turn the vortex flow, and (iii) reconvert it into a uniform parallel flow at the airfoil exit. Several airfoil geometries were designed with varying exit Mach numbers.

The planned design method has been assessed using three dimensional Navier–Stokes simulations. The computational grid was first carefully selected to ensure a grid independent solution based on the CGI method. The simulations comprised steady and unsteady-transient analysis. The results showed the ability of the present design to ingest normal shock waves, allowing the passage to operate in the supersonic regime. Furthermore, the coupled analysis of the density gradient contours together with the pressure losses revealed the prime source of loss attributed to the leading edge shock reflections across the turbine passage. The developed design tool allows producing turbine passages twice more efficient than the current state-of-the-art turbine designs.

The aerodynamic presentation of a stator less turbine was analyzed at several incidence angles. Severe pressure abatement is observed due to shock losses and secondary flows. At high incidence, a separation bubble on the suction side creates significant losses. In contrast to subsonic turbines the static pressure increases along the turbine. In spite of the limited turning, large values of power are extracted. Furthermore, the starting phase from stagnation to supersonic regime was analyzed with a transient simulation, complex shock patterns develop during the ingestion of normal shock waves, which typically last for about 30 ms. Fluid machinery designers are usually constrained to operate in the subsonic regime, however the present design approach opens avenues for the development of revolutionary ultra compact power generation concepts.

### References

1. Joly M, Verstraete T, Paniagua G. Multidisciplinary design optimization of a compact highly-loaded fan. Structural and Multidisciplinary Optimization. Journal of the International Society for Structural and Multidisciplinary Optimization. Published online: 25 August 2013. StructMultidiscOptim1615-147X2013. <http://dx.doi.org/10.1007/s00158-013-0987-5> (August).

2. Goldman LJ, Vanco MR. Computer Program for Design of Two-Dimensional Sharp-Edged-Throat Supersonic Nozzles with Boundary-Layer Correction. NASA Technical Memorandum, TM X-2343, Published by National Aeronautics and Space Administration, Lewis research center, Cleveland, Ohio
3. Roy GD, Frolov SM, Borisov AA, Netzer DW. Pulse detonation propulsion: challenges, current status, and future perspective. Prog Energy CombustSci0360- 1285 2004; 30(6):545–672. <http://dx.doi.org/10.1016/j.pecs.2004.05.001>.
4. Kantrowitz A, Donaldson CD. Preliminary Investigations of Supersonic Diffusers. (NACA Report ACR-L5D20). Langley Field, VA: Langley Memorial Aeronautical Laboratory; 1945.
5. Celik IB, Ghia U, Roache PJ, Freitas CJ, Coleman H, Raad PE. Procedure for estimation and reporting of uncertainty due to discretization in CFD applications. ASME J Fluids Eng 0098-2202 2008; 130(078001):4. <http://dx.doi.org/10.1115/1.2960953>

